J. Membrane Biol. 84, 269–283 (1985)

The Journal of
Membrane Biology

Permeability Properties of Cell-to-Cell Channels: Kinetics of Fluorescent Tracer Diffusion through a Cell Junction

A.L. Zimmerman* and B. Rose
Department of Physiology and Biophysics, University of Miami School of Medicine, Miami, Florida 33101

Summary. We have analyzed the intracellular and cell-to-cell diffusion kinetics of fluorescent tracers in the *Chironomus* salivary gland. We use this analysis to investigate whether membrane potential-induced changes in junctional permeability are accompanied by changes in cell-to-cell channel selectivity. Tracers of different size and fluorescence wavelength were coinjected into a cell, and the fluorescence was monitored in this cell and an adjacent one. Rate constants, k_J, for cell-to-cell diffusion were derived by compartment model analysis, taking into account (i) cell-to-cell diffusion of the tracers; (ii) their loss from the cells; (iii) their binding (sequestration) to cytoplasmic components; and (iv) their relative mobility to cytoplasm, as determined separately on isolated cells. In cell pairs, we compared a tracer's k_J with the electrical cell-to-cell conductance, g_J.

At cell membrane resting potential, the k_J's ranged 3.8–9.2 $\times 10^{-3}$ sec^{-1} for the small carboxyfluorescein (mol wt 376) to about 0.4 $\times 10^{-3}$ sec^{-1} for a large fluorescein-labeled sugar (mol wt 2327). Cell membrane depolarization reversibly reduced g_J and k_J for a large and a small tracer, all in the same proportion. This suggests that membrane potential controls the number of open channels, rather than their effective pore diameter or selectivity. From the inverse relation between tracer mean diameter and relative k_J we calculate an effective, permeation-limiting diameter of approximately 29 Å for the insect cell-to-cell channel.

*Intra*cellular diffusion was faster than cell-to-cell diffusion, and it was not solely dependent on tracer size. Rate constants for intracellular sequestration and loss through nonjunctional membrane were large enough to become rate-limiting for cell-to-cell tracer diffusion at low junctional permeabilities.

Key Words cell-to-cell channels · junctional permeability · gap junction · intercellular communication

Introduction

In many tissues, cells are interconnected by cell-to-cell channels that provide a direct link between the cells' interiors (Loewenstein, 1981). In insect cells, the channels' effective, permeation-limiting diameter was estimated at 20 to 30 Å, and in mammalian cells, at 16 to 20 Å (Schwarzmann, Wiegandt, Rose, Zimmerman, Ben-Haim & Loewenstein, 1981). Cell-to-cell channels thus constitute intercellular pathways not only for small inorganic ions but also for a large variety of organic molecules.

The permeability of cell junctions is affected by a variety of cell treatments, such as changing the cytoplasmic *p*Ca (Oliveira-Castro & Loewenstein, 1971; Rose & Loewenstein, 1975, 1976; Dahl & Isenberg, 1980) or pH (Turin & Warner, 1977, 1980; Rose & Rick, 1978; Spray, Harris & Bennett, 1981*a*) or, in one tissue, changing the cells' membrane potential (Rose, 1970; Socolar & Politoff, 1971; Obaid, Socolar & Rose, 1983), and in others, changing the trans-channel potential (Spray, Harris & Bennett, 1979, 1981*b*; Harris, Spray & Bennett, 1981).

In this study on insect (*Chironomus thumni*) cell junctions, we probed the cell-to-cell channels' permeability with several fluorescent tracers of different sizes. We measured the kinetics of the fluorescence changes in the tracer-injected cell and an immediate cell neighbor. Using a compartment model, we analyzed these kinetics in terms of their following underlying components: the tracers' cell-to-cell diffusion, their loss through nonjunctional membrane, and their intracellular diffusion and sequestration. We derived rate constants, k_J, for the cell-to-cell diffusion of the tracers—a parameter that reflects exclusively junctional permeability.

We use this analysis for k_J—to study the nature of the changes in junctional permeability induced by shifts in cell membrane potential. In particular, we ask whether changes in junctional permeability entail transitions of the cell-to-cell channels only between open and closed states or also transitions between stable open states that differ in effective pore diameter, as previously proposed (Rose, Simpson & Loewenstein, 1977; Loewenstein, Kanno & So-

* *Present address:* Department of Neurobiology, Sherman Fairchild Science Building, Stanford University School of Medicine, Stanford, California 94305.

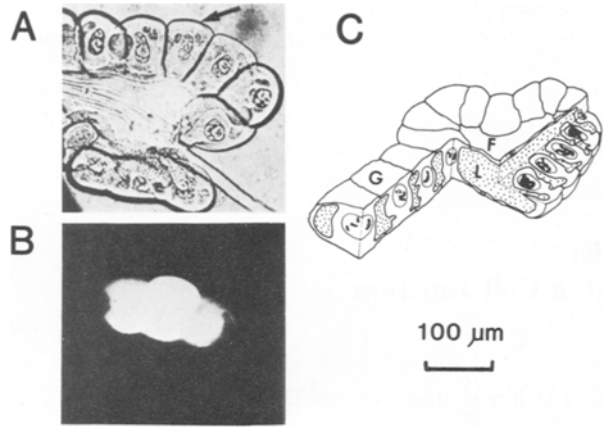

Fig. 1. The *Chironomus* salivary gland. (*A*) Brightfield and (*B*) fluorescence images of the giant cells. Rows of cells like those in the top row were typically chosen for the experiments. The cells in such rows were of approximately the same size and shape and had distinct, nonoverlapping borders. Arrow indicates cell injected with a fluorescent tracer. (*C*) Schematic drawing of the gland: central lumen (*L*), giant cells (*G*), flat cells (*F*) forming the roof and floor of the gland. (Part *C* reprinted with permission from Rose, 1971)

colar, 1978). A change in pore diameter would be expected to result in a change in the ratio of the junctional permeabilities, i.e., of the k_J values, for permeants of different sizes.

We find that shifts in membrane potential effect proportional changes in K_J for a small and a large tracer, as well as in the electrical conductance changes in junctional permeability do not entail changes in selectivity or effective pore diameter of open cell-to-cell channels. From the inverse relation between k_J and permeant size, we calculate this diameter to be approximately 29 Å.

Materials and Methods

The Cellular Preparations and Media

Salivary glands (Fig. 1) were obtained from fourth instar larvae of the midge *Chironomus thummi,* by removal of the head and esophagus, and subsequent detachment of the glands. They were placed into plastic petri dishes and, unless stated otherwise, superfused continuously with an insect saline, *CHEER* [in mM: KCl, 2; NaCl, 28; Na_2-fumarate, 28; $CaCl_2$, 5; Mg-succinate, 7;

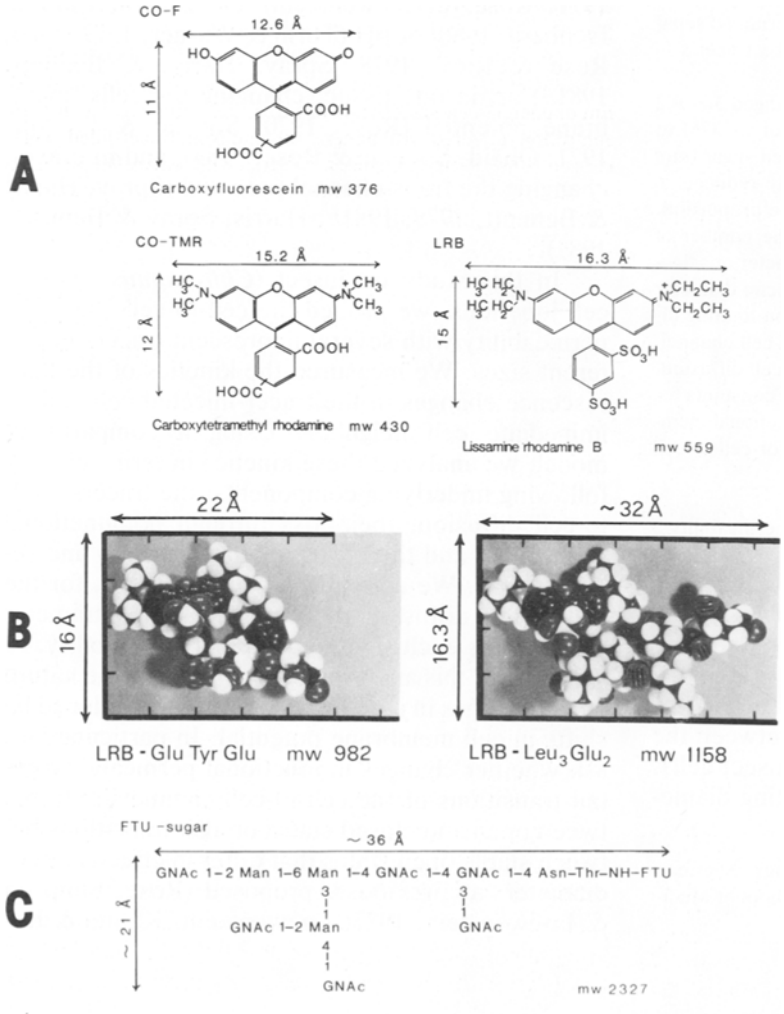

Fig. 2. Fluorescent tracers. (*A*) Chemical structures of the fluorophores. (*B*) Space-filling (Corey-Pauling-Koltum) models of the two LRB-labeled peptides. (*C*) Chemical composition of the fluorescein-labeled glycopeptide FTU-sugar. Arrow bars give the tracers' two largest dimensions, as determined from the models

glutamine, 80; TES, 5; titrated to pH 7.4 with NaOH, 4 to 5 (Politoff, Socolar & Loewenstein, 1969)].

A gland consists of about 30 giant (*G*) cells—the cells we used for injection in our experiments—surrounding a lumen whose roof and floor are formed by several broad, flat (*F*) cells (Fig. 1; Rose, 1971). Commonly, a few *G* cells and *F* cells in each gland did not survive the dissection procedure, but each *G* cell chosen for tracer injection had at least two healthy *G* neighbors on either side. Although the *F* cells make gap junctions with the *G* cells and are electrically coupled to them (Rose, 1971), in the present studies, tracer injected into a *G* cell never spread detectably into *F* cells or via *F* cells into other *G* cells—nor into injured cells. Presumably, the number of cell-to-cell channels connecting *F* to *G* cells is only a small fraction of that connecting *G* cells (*see also* Metzger & Weingart, 1984). We therefore considered these "gland" preparations in effect as chains of 5–7 cells and base our analysis of the data on this simple geometry (*see* Results, p. 275, and Appendix).

Single cells and cell pairs were obtained by dissecting away or injuring neighboring cells. In some experiments, cell pairs were isolated by enzyme treatment (Obaid et al., 1983) and transferred to an insect tissue culture medium (TC-199MK), a mixture of TC-199 (GIBCO medium 199, Hank's salts) and *Melnick's* medium (in mM: NaCl, 136.9; KCl, 5.36; $CaCl_2$, 1.76; $MgSO_4$, 0.46; $MgCl_2$, 0.49; $NaHPO_4$, 0.44; dextrose, 5.55; lactalbumin hydrolysate, 10 g/liter), with L-glutamine and fetal calf serum added to yield a final concentration of 2 mM and 10%, respectively, and adjusted to pH 7.2 with NaOH.

All experiments were performed at room temperature.

Measurement and Control of Membrane Potential

Membrane potential was measured with 20 to 50 MΩ microelectrodes filled with 0.5 M K_2SO_4. Membrane potential was changed by varying extracellular $[K^+]$: TC-199MK or CHEER was replaced by or mixed with, respectively, *K-Melnick's* (Melnick's medium with all Na replaced with K) or *K-CHEER* (in mM: KCl, 30; $CaCl_2$, 5; Mg-succinate, 7; glutamine, 80; KH-fumarate, 28; KOH, 32; pH 7.4).

In some experiments on isolated cell pairs, a double voltage clamp (Obaid et al., 1983) was used to control membrane potential and to measure junctional conductance. For this, each cell of a pair was impaled with a voltage-sensing and a separate current-passing electrode, and both cells were clamped independently to the same membrane potential. Small square voltage pulses ΔE_1 (2 to 5 mV, 1 to 2 sec) were then applied to one cell of the pair, and junctional conductance, g_J, was calculated as $-\Delta i_2/\Delta E_1$, where Δi_2 is the resulting change in clamp current of the other cell (equal but opposite in sign to the current passing through the junction) during ΔE_1.

Resting membrane potentials of cells in CHEER or in TC199-MK ranged −25 to −45 mV.

Fluorescent Tracer Molecules

The following fluorescent tracers were used: Carboxyfluorescein (CO-F, Eastman Kodak), lissamine rhodamine B (LRB, Molecular Probes, Inc.), LRB-labeled peptides LRB-Glu-Tyr-Glu and LRB-Leu_3Glu_2, and a branched sugar labeled with fluorescein (FTU-sugar). Figure 2 presents the molecular weight, structure, and two largest dimensions of each tracer. Preparations of the tracers are described by Simpson, Rose and Loewenstein (1977), and Schwarzmann et al. (1981). All tracers were dissolved in 0.1 M HEPES, pH 7.4, at concentrations of 2 to 10 mM, and stored frozen. Tracer purity was tested by paper electrophoresis. Tracers were backfilled into thin-walled glass micropipettes (Ultratip, Frederick Haer, Inc.) of 5 to 10 MΩ resistance (when filled with 0.5 M K_2SO_4) and injected into cells by pulsed gas pressure.

Fluorescence Measurements

We used a Leitz Ortholux II microscope equipped with incident-light illumination (ploemopak; HBO 100W mercury arc lamp) and a 50× water immersion objective (numerical aperture, 0.9; free working distance, 0.75 mm). A multi-wavelength microfluorometer (Johnson Foundation, Philadelphia) was coupled by means of waveguides to the microscope (Fig. 3). This system allowed us to measure nearly simultaneously the fluorescence emission from two different tracers (e.g., red from rhodamine and green from fluorescein) at two sites. The four photocurrent outputs were converted to voltages and recorded on a Soltec strip chart recorder.

Before the start of experiments, the gains of the four outputs were adjusted so that equal outputs were obtained from both recording sites at equal concentrations of both tracers. The amplitudes of the fluorescence signals for co-injected tracers can thus be directly compared. For this calibration, we used 200 μl drops of tracer solutions of known concentrations (in 0.1 M HEPES, pH 7.4). The relation between fluorescence intensity and tracer concentration was linear between 0.1 and 25 μM. At higher concentrations, saturation occurred.

To relate fluorescence intensity to actual intracellular tracer concentration, we measured the fluorescence from individual 100 μm diameter (cell-size) drops of tracer solutions of known concentration, covered with mineral oil, and from tracer-filled capillaries of 100 μm inner diameter, covered with water. On the basis of these measurements we kept the intracellular concentration of tracers in the linear range: the peak fluorescence intensity in the injected cells corresponds to tracer concentrations between 10–25 μM.

For the measurements of tracer diffusion in agar, drops of 0.5% agar in distilled water and of roughly 100 μm diameter were prepared, allowed to solidify, and covered with mineral oil.

Results

A. Intracellular Tracer Diffusion (Measurements on Single Cells)

To obtain a measure of the relative mobility of the various tracers in the cytoplasm, a mixture of two tracers was injected at one end of the cell, and the resulting fluorescence changes were recorded at this (*F*1) and the other end (*F*2) of the cell (single cell, isolated from the gland). Figure 4*A* illustrates typical data for carboxyfluorescein (CO-F). The data for LRB, co-injected with CO-F—molecules of rather similar size and shape—are shown in Fig. 4*B* (solid lines), superimposed on the CO-F data (dotted curves) which were scaled here to peak *F*1 of the LRB data. LRB is clearly less mobile inside the

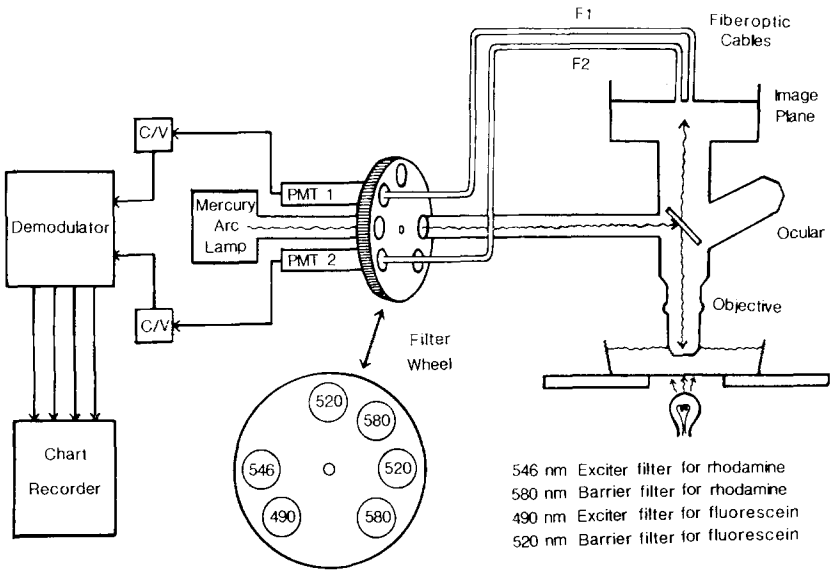

Fig. 3. Fluorimetric system. Exciting light travels from the mercury arc lamp through an exciter filter in a rotating filter wheel to the microscope. There it is deflected by a dichroic mirror to the preparation through a 50× salt water immersion objective. Emitted fluorescence is transmitted through the dichroic mirror to collecting fiberoptic cables positioned at the image plane in a lightproof box above the microscope. Fluorescence collected from two locations is carried to photomultiplier tubes (*PMT*'s *1* and *2*) through appropriate barrier filters in the wheel. The output from each PMT is sent through a current-to-voltage converter (*C/V*) to the demodulator for sorting, amplification, and equalization (*see* Materials and Methods) and then to a chart recorder. The air-driven filter wheel spins at about 70 Hz, allowing the recording of two fluorescence wavelengths in rapid succession. An electronic encoder in the axle allows signal sorting. Transmitted light from a tungsten-halogen lamp is used for brightfield observation in between measuring periods

cell than CO-F; the *F*1 peak occurs later, and the lag to rise in *F*2 is more pronounced. Furthermore, tracer equilibration takes 2.4 times longer for LRB than for CO-F: half-times for approximate equilibration (when *F*1 and *F*2 are roughly equal and decaying together) were 12.6 sec for CO-F and 30.6 sec for LRB.

In agar, on the other hand, the diffusion rates for the two similarly sized molecules are comparable (Fig. 4*D*): the half-times for approximate *F*1, *F*2 equilibration are 3.5 sec for CO-F and 4.7 sec for LRB, differing by a factor of only 1.3.

Thus, molecular size seems not to be the reason for the slow cytoplasmic diffusion of LRB. In fact, the much larger peptides labeled with LRB exhibited about the same intracellular mobility relative to CO-F as did LRB alone: equilibration of LRB-Glu-Tyr-Glu (mol wt 982), e.g., was about 2.33 times that of co-injected CO-F (not shown). Diffusion of carboxytetramethyl rhodamine (CO-TMR, mol wt 430), on the other hand, closely resembled that of CO-F: half-time to *F*1, *F*2 equilibration (15 sec) was 1.2 times that for co-injected CO-F.

B. Fluorescence Loss and Tracer Sequestration

The slow and parallel decay of fluorescence intensity at both recording sites after *F*1 and *F*2 equilibration (seen most clearly in Fig. 4*C*) represents an overall loss of fluorescence from the cell. The rate of loss differed for the tracers, being lowest for the LRB group. Such a loss could be due to photodecomposition, to leakage through the plasma membrane, or to uptake into some cellular compartment, with subsequent quenching or exocytosis.

Photodecomposition was negligible: the fluorescence from tracers injected into an agar drop under mineral oil decayed with a similar time course in the presence or absence of exciting light. Fluorescence loss here must have been due mainly to diffusion of tracer from the agar into the oil. The tracers lost most slowly from agar drops, LRB and LRB-Glu-Tyr-Glu, were also lost most slowly from cells, perhaps reflecting a lower lipid solubility, and hence a lower (nonjunctional) membrane permeability.

It was often evident that the tracers were sequestered in the cells and seemingly taken up into intracellular compartments, probably vesicles: brightly fluorescent spots became discernible near the surface of injected cells (Fig. 5*B*), in some experiments as soon as 20 min after injection, but not at all in others.

On changing the focus, some spots appeared to dangle from the cell surface as if attached by fine strands, giving the impression of being extruded from the cell. When two different tracers were injected, the spots fluoresced both red and green, in-

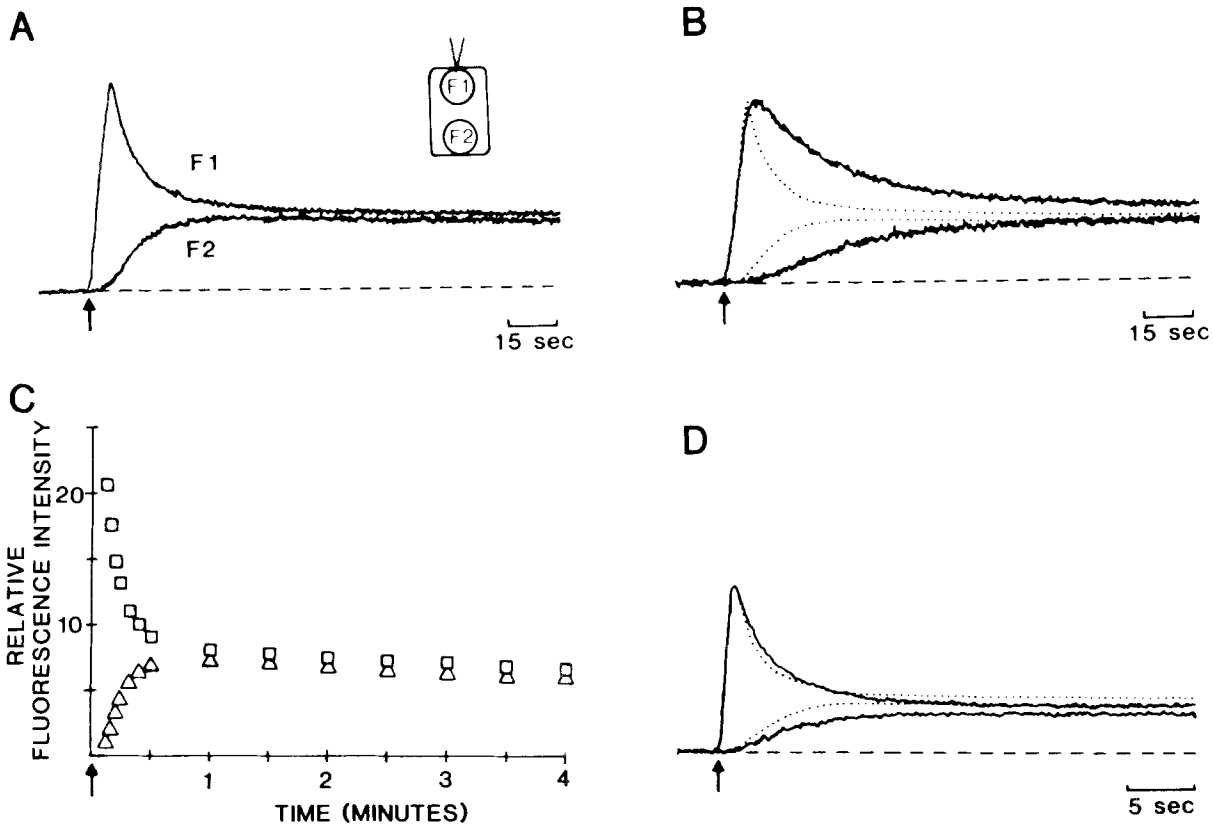

Fig. 4. Diffusion of CO-F and LRB in cytoplasm and in agar. (*A*, *B*) Chart recordings of the fluorescence intensities at two sites, *F1* and *F2*, inside an isolated cell. *F1*, the site of injection, is at one end of the cell; *F2* is at the other. The inset in this and other figures indicates the fiberoptic cables' positions over the cell image(s) and their approximate relative size. Arrows denote tracer injection. Simultaneous records for CO-F (*A*) and LRB (*B*). The dotted lines in *B* are the data in *A*, scaled to the peak *F1* fluorescence of LRB. (*C*) Plot of the data in *A*, for a longer period. The ordinates in this plot of relative fluorescence intensity—and in such plots in the following figures—are the actual photovoltages recorded in the respective experiment and are proportional to tracer concentration. (*D*) Diffusion in 0.5% agar: LRB (solid lines) and CO-F (dotted, scaled to peak *F1* of LRB). Note the different time scales

dicating that both tracers were being sequestered in the same compartment, although perhaps not necessarily to the same degree. This sequestration was probably not due to injury from injection, because the spots could also be seen in the adjacent cells.

C. Cell-to-Cell Diffusion. Comparison of Tracers' Junctional Permeabilities by Compartment Model Analysis of Cell-to-Cell Diffusion Kinetics

Figure 6 shows the time course of fluorescence intensity changes in a cell injected with CO-TMR (*F1*) and in an adjacent one (*F2*). The initial, rapid decay of *F1* during the first half minute after injection can be attributed to diffusion of the tracer within the cell; the decay rate is comparable to that at the injection site of an isolated cell (Fig. 4*A*), and diminishes with increasing distance from the injection site (*see* Fig. 7). As in single cells, both the rise to peak and the rate of decay are slower for LRB and the LRB-labeled tracers than for the other tracers

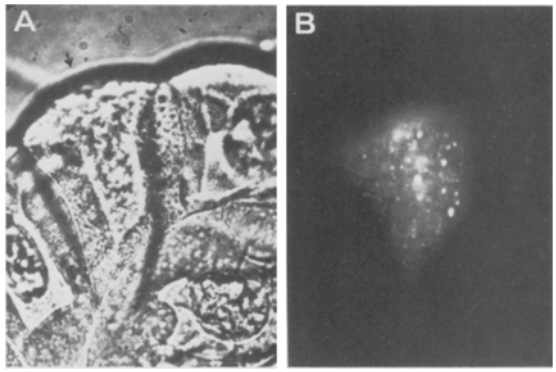

Fig. 5. Tracer sequestration in the cells. Brightfield (*A*) and fluorescence (*B*) images of a cell injected with carboxy tetramethylrhodamine (CO-TMR) and fluorescein isothiocyanate-Glu-Tyr-Glu. Photographs were taken about 1.5 hr after injection, with the optics focused on the surface of the cell

used (*compare* the first minute of Fig. 8*B*, LRB-Glu-Tyr-Glu, with Fig. 6, CO-TMR, and with Fig. 8*A*, CO-F). The subsequent and much slower *F1* decay and concomitant *F2* rise reflect predomi-

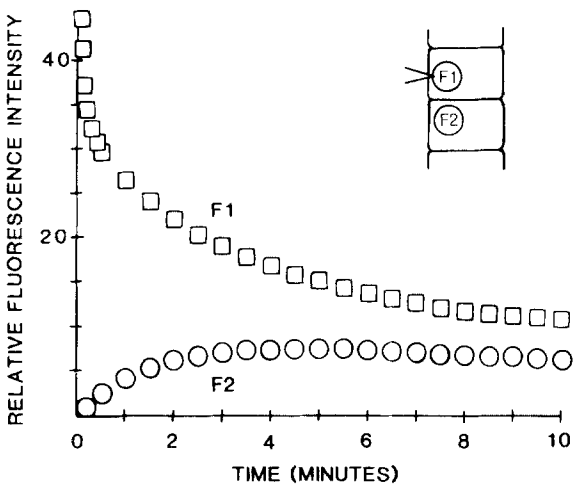

Fig. 6. Cell-to-Cell diffusion of CO-TMR. Fluorescence in the injected cell (*F1*, squares) and an immediate neighbor (*F2*, circles), at resting potential, −28 mV (measured in the injected cell). Gland in CHEER, 2 mM K. Tracer injection at time zero

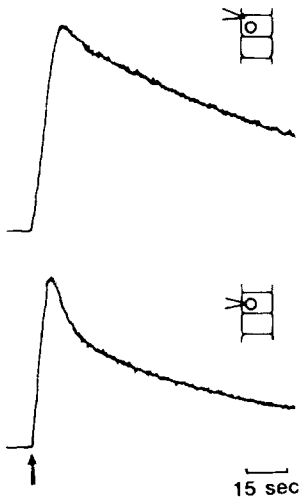

Fig. 7. Fluorescence recordings in injected cell at different locations with respect to injection site. In the experiment of the upper record, the injection pipette was outside the recording field, in that of the lower, inside

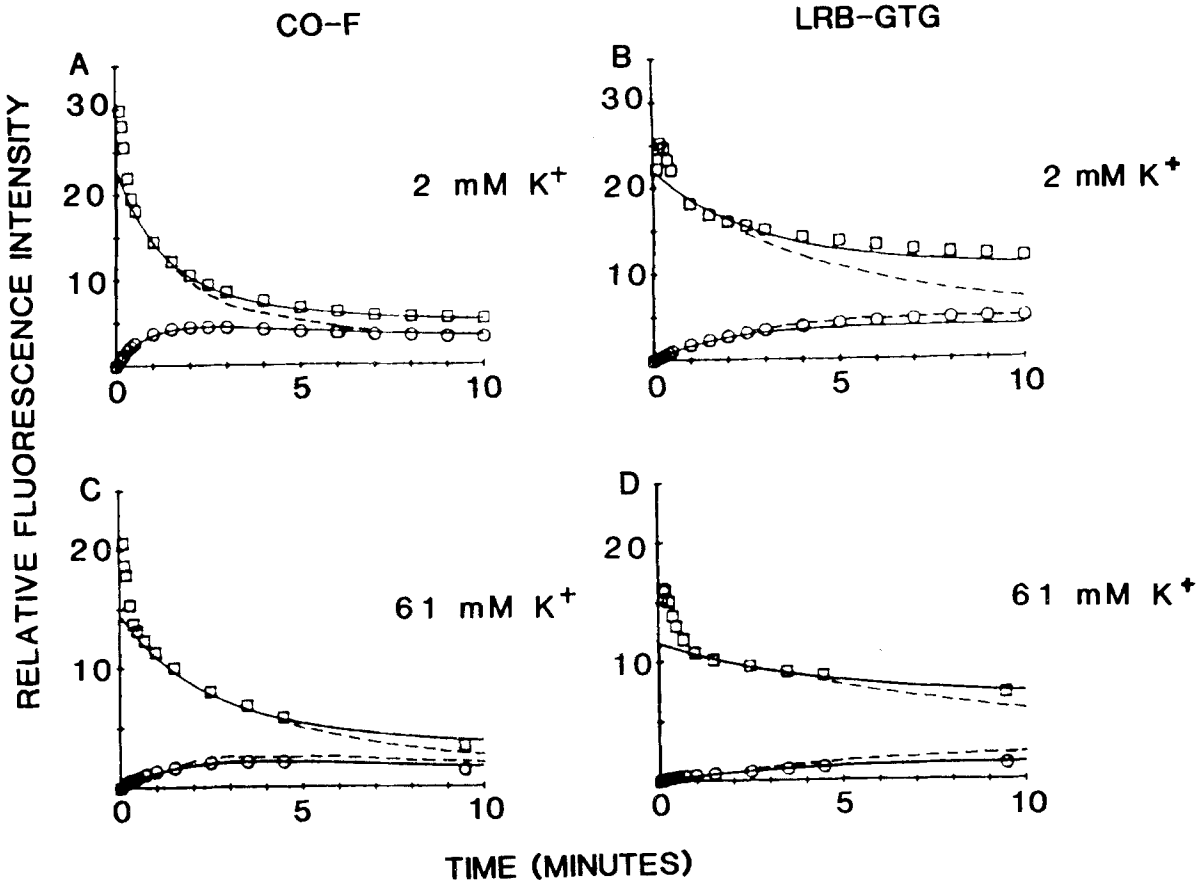

Fig. 8. (*A* and *B*): Cell-to-cell diffusion of tracers of different sizes. (*C* and *D*): Reduction by membrane depolarization (CO-F, left; LRB-Glu-Tyr-Glu, right); comparison by compartmental analysis. Squares (*F1*) and circles (*F2*) are experimental data of fluorescence intensities; solid and dashed lines are theoretical curves of the tracer concentrations according to the compartmental analysis, using the parameters described below. (*A* and *B*) gland in 2 mM K, (*C* and *D*) in 61 mM K (K-CHEER : CHEER, 2 : 1). Parameters k_J, k_L, k_S for the theoretical curves (solid lines), respectively (rate constants, 10^{-3} sec^{-1}): (*A*): 8.7, 0.67, 1.0; (*B*): 3.0, 0.83, 1.83; (*C*): 4.0, 1.17, 1.0; (*D*): 1.38, 0.15, 1.83. For the dashed curves, k_S was zero; k_J and k_L were, respectively: (*A*): 8.7, 0.67; (*B*): 3.0, 0.083; (*C*): 4.0, 0.67; (*D*): 1.38, 0.083

nantly cell-to-cell diffusion. The final slow and parallel decay of $F1$ and $F2$ can be attributed to tracer loss from the cells, as its kinetics are similar to the net fluorescence loss seen in single cell experiments. In some experiments (not shown), $F1$ and $F2$ were equal in amplitude during this slow decay phase.

For a direct comparison of the cell-to-cell diffusibility of tracers of different sizes through a particular junction, we co-injected tracer pairs into a cell. The result of such an experiment is shown in Fig. 8*A* and *B*, in which CO-F (mol wt 376) was co-injected with LRB-Glu-Tyr-Glu (mol wt 982). The cell-to-cell diffusion kinetics are clearly slower for the larger tracer. To derive from these data a parameter, k_J, that specifically and exclusively reflects the junctional permeability of the tracer in question, we analyzed the kinetics using a compartment model.

In our model the cells of a five-cell chain are represented as identical, serially interconnected compartments, each containing a subcompartment representing the irreversible sequestration of tracer (*see* Fig. 9). Compartment-to-compartment (cell-to-cell) transfer, irreversible sequestration, and loss of tracer from a compartment are assumed to be linear, first-order processes and are represented by rate constants k_J, k_S, and k_L, respectively. Sequestered tracer is assumed to contribute to fluorescence (*see*, e.g., Fig. 5). Based on this model, the time course of the changes in concentration of tracer, injected into the middle compartment, is computed for this and a neighboring compartment and, by the appropriate choice of the rate constants, is fitted to the experimental data of $F1$ and $F2$. (The model is described in detail in the Appendix; *see* Riggs (1963) for a general description of compartmental analysis.)

To simplify the mathematical treatment, we did not include intracellular diffusion in the model. A formal theoretical treatment of intracellular diffusion would involve many assumptions concerning the complex shape of the cells (Fig. 1) and yield an intractable set of differential equations. Instead, since our experiments on isolated cells indicate that dispersion of tracer throughout the cell (initial rapid $F1$ decay) is complete within the first 0.5 to 1.0 min after injection (depending on the tracer), we fitted the simulations to the $F1$ data accordingly, starting, e.g., at 0.5 min for CO-F and at 1.0 min for LRB-Glu-Tyr-Glu.

The solid curves in Fig. 8 were generated using this model. They agree reasonably well with the data (symbols) after the initial rapid $F1$ decay phases. In Fig. 8*A* and *B* the junctional diffusion rate constant k_J was set at 8.7×10^{-3} sec^{-1} for CO-F, and 3.0×10^{-3} sec^{-1} for LRB-Glu-Tyr-Glu, suggesting a roughly threefold higher junctional permeability for CO-F than for LRB-Glu-Tyr-Glu. Figure 10 shows data and theoretical curves for FTU-sugar (mol wt 2327), a molecule apparently close to the limit of channel permeation. Here, a k_J of 0.42×10^{-3} sec^{-1} gave a good fit to the data. Table 1 presents the results of comparing theoretical curves with fluorescence data from six injection trials (six different junctions) for five tracers. It is evident that k_J varies inversely with tracer size, and that tracer net negative charge is not a major determinant of k_J. (These data are from the paired injections listed in Table 2.)

D. Effect of Cell Membrane Potential on Cell-to-Cell Tracer Diffusion. Does Depolarization Change Cell-to-Cell Channel Selectivity?

Cell depolarization by exposure to high extracellular [K^+], a treatment known to reduce junctional

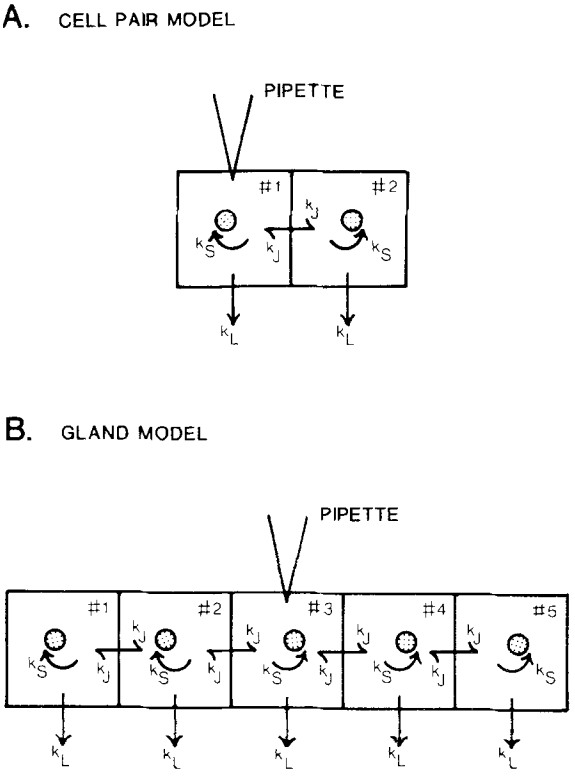

Fig. 9. The compartment model used in analyzing cell-to-cell diffusion data. Cells are represented as identical compartments in series (the numbers identify the individual compartments in the differential equations in the Appendix). Tracer molecules are assumed to: spread from cell to cell through junctional channels (rate constant, k_J); be irreversibly lost from the cells or become nonfluorescent (rate constant, k_L); or be irreversibly sequestered into vesicles or other cellular compartments (dotted circles; rate constant, k_S), where they remain fluorescent but are not free to diffuse through cell-to-cell channels. (*A*) The cell-pair and (*B*) the "gland" (five-cell chain) version of the model

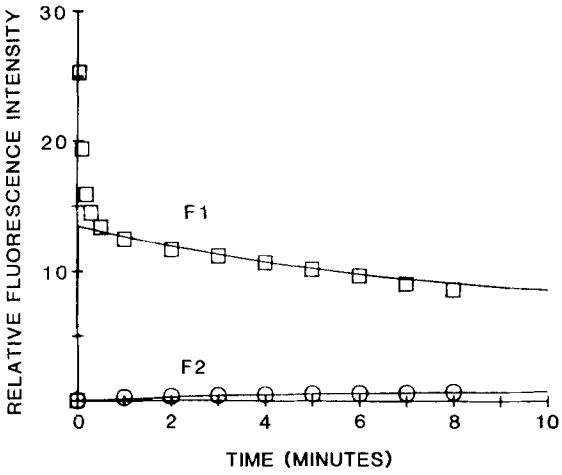

Fig. 10. Cell-to-cell diffusion of a large tracer close to the limit of permeation. At time zero, the fluorescein-labeled glycopeptide FTU-sugar (mol wt 2327) was injected into a cell in a gland in 2 mM K^+, membrane potential, −36 mV. Symbols are experimental data of fluorescence intensity, and curves are as calculated using the compartment model described in the Appendix; the rate constants for these curves are (10^{-3} sec^{-1}): k_J, 0.42; k_L, 0.67; k_S, 1.0

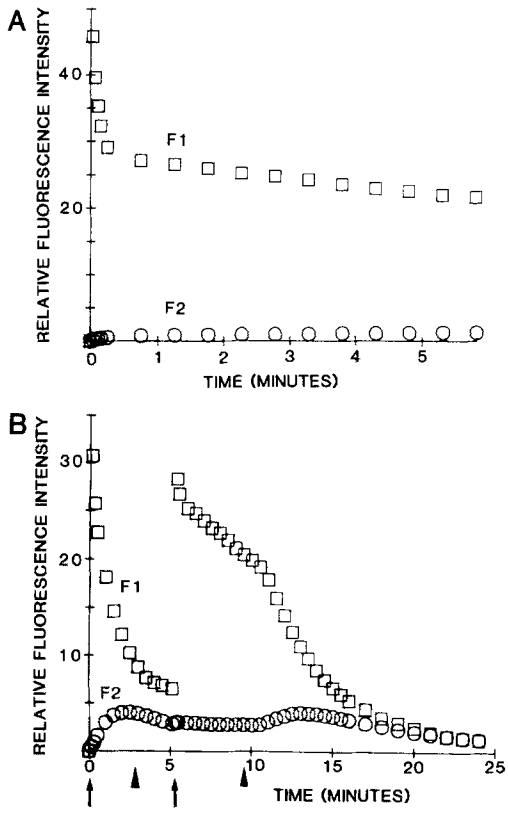

Fig. 11. Reduction of cell-to-cell tracer diffusion by cell depolarization. (*A*): Fluorescence data from a CO-TMR injection into the same cell as in Fig. 6, but the gland is in 46 mM K^+ (CHEER/K-CHEER, 1 : 1) which depolarized the cell(s) to −18 mV (measured in injected cell). (*B*): Reversibility. At time zero (first arrow), carboxy fluorescein (CO-F) is injected into a cell of a gland in 2 mM K^+. The medium is then changed (first triangle) to 90 mM K^+ (K-CHEER); this depolarizes cells to −8 to 0 mV, as measured not here but in many other experiments. The *F*1 decay in 90 mM K^+ is slower than in 2 mM K^+, and *F*2 does not rise, indicating marked reduction of cell-to-cell diffusion. At the second arrowhead, the medium is changed back to 2 mM K^+, and the *F*1 decay rate increases abruptly and *F*2 rises. The 1-min lag of these responses corresponds to the lagtime of the exchange of medium in the bath

conductance in these cells (Obaid & Rose, 1981; Obaid et al., 1983), also reduced cell-to-cell tracer diffusion. Figure 11*A* illustrates this for the same cells as those in Fig. 6, but after cell membrane potentials were lowered from −28 to −18 mV by increasing extracellular [K^+]. Whereas the initial *F*1 decay remains unchanged, the later *F*1 decay and the *F*2 rise are markedly slowed—in fact, *F*2 barely rises at all. This depression of cell-to-cell transfer is reversed on returning to the normal, 2 mM [K^+], as shown in Fig. 11*B*. Here, two injections were done, the first (first arrow) with the cells in 2 mM [K^+], and the second (second arrow) in 90 mM [K^+]. While in high [K^+], *F*2 shows no rise on injection, and *F*1 decays slowly. Upon return to 2 mM [K^+] (second arrowhead), junctional permeability is increased, as shown by the rapid fall in *F*1 and concomitant rise in *F*2.

To determine whether depolarization changes channel selectivity, we compared the cell-to-cell diffusion kinetics of tracers of different sizes, co-injected at cell resting potential and at a more positive potential. Figure 8 shows such an experiment, in which two co-injections of LRB-Glu-Tyr-Glu (mol wt 982) and CO-F (mol wt 376) were made, one with the preparation in 2 mM K^+ (*A* and *B*), another in 61 mM K^+ (*C* and *D*). Cell-to-cell diffusion of both the large and the small tracer is depressed in the high K medium. This result is representative of 25 experiments carried out at various K concentrations. In extreme cases, cell-to-cell diffusion of both tracers was so severely reduced that *F*2 was just barely detectable for the smaller tracer, and undetectable for the larger one (not illustrated). Clearly, depolarization slows the cell-to-cell diffusion of both large and small tracers. The question is, however, whether the junctional permeability of both tracers is reduced equally. The result from compartmental analysis suggests it is. In the control condition (2 mM K, Fig. 8*A* and *B*), k_J for the theoretical curves was 8.67×10^{-3} sec^{-1} for CO-F, and 3.0×10^{-3} sec^{-1} for LRB-Glu-Tyr-Glu, and when the cells were depolarized (61 mM K, Fig. 8 *C* and *D*), k_J for the theoretical curves was 4.0 and 1.38×10^{-3} sec^{-1} for CO-F and LRB-Glu-Tyr-Glu, respectively. In other words, a reduction in k_J (i.e., in junctional permeability) by a factor of 2.17 for both tracers

Table 1. Relation of k_J to tracer size and charge

Tracer	mol wt	Net negative charge at pH 7	Mean diameter[a] (Å)	k_J(max) × 10^3 (sec $^{-1}$)	Percent of k_J (CO-F)
CO-Fluorescein	376	1–2	10.35	9.17	100
CO-Tetramethylrhodamine	430	1	11.34	5.83	63.6[b]
LRB-Glu-Tyr-Glu	982	3	15.40	3.06	33.5 ± 1.9(3)[c]
LRB-Leu_3-Glu_2	1158	3	16.74	1.3	14.7 ± 0.5(2)[c]
FTU-sugar	2327	1	23.87	0.42	4.6[b]

[a] Defined as the geometric mean diameter, $\sqrt[3]{l \cdot w \cdot d}$, of the smallest rectangular box of length l, width w, depth d, into which a space-filling (Corey-Pauling-Koltum) model of the particular tracer could be fit.

[b] Data from injection #6, Table 2; CO-F was not co-injected here.

[c] Percent of co-injected k_J(CO-F) ± SD; in parenthesis, number of experiments; data from cells at resting potential (injection #s 1*a*, 2–5, Table 2).

could account for their altered diffusion kinetics in the depolarized cells.

For the simulations in Fig. 8, tracer sequestration was assumed to occur, and tracer loss was assumed to be greater for the second than for the first injection (although proportionately increased for both tracers). Inclusion of these assumptions tightened the correspondence between theoretical curves and data at late times. This can be seen by comparing (Fig. 8) the solid curves with the dashed ones for which no sequestration is assumed (k_S = 0), and k_L is held constant. The main result of sequestration is to cause $F1$ and $F2$ to level out sooner. LRB-Glu-Tyr-Glu was assigned a larger k_S and a smaller k_L than was CO-F—a reasonable assumption in the light of our results with single, isolated cells, which suggested greater binding and slower loss for the former tracer. The assumption that tracer loss is increased by the second injection (40 min after the first one) is also reasonable, since a decline in input resistance and eventually a swelling of cells were sometimes observed during long experiments. However, consistent with the variability in appearance of bright spots (Fig. 5) and in loss of input resistance, it was not always necessary to include sequestration and an increase in tracer loss for simulating such data.

It was not possible to simulate the effects of depolarization on both $F1$ *and* $F2$ by changing k_L and/or k_S without changing k_J. An increase in k_L and/or k_S can account for a lower peak $F2$, but it cannot mimic the observed changes in kinetics of $F1$ and $F2$: a larger k_L produces an increase in the rate of $F1$ decay instead of the decrease actually seen with depolarization; and as evident in Fig. 8, increasing k_S has no effect on the initial rate of rise of $F2$, whereas this rate is slowed considerably in depolarized cells. A fit to both $F1$ *and* $F2$ thus places severe constraints on the choice of rate constants in these simulations. Varying k_J by more than 10 to 20% gave substantially worse fits than those illustrated in Fig. 8.

The summary of the analyses shown in Table 2 highlights the main results obtained from these experiments. First, k_J for a given tracer varies from junction to junction (*compare* injections 1*a*, 2, 3, 4, and 5 for CO-F). Second, for a given junction and a given tracer, k_J decreases with increasing K^+ concentration (i.e., with decreasing cell membrane potential; *compare* injections 1*a* and *b*, 7*a* and *b*[1]). Third, although the absolute values of k_J for co-injected tracers vary, their ratio (e.g., k_J(CO-F)/k_J(LRB-Glu-Tyr-Glu)) remains constant within 11% (*compare* injections 1, 2, 3, and 4, 5), well within our experimental and simulation errors. This implies that the relative junctional permeability of the tracer pairs is the same in the various junctions and is maintained on depolarization.

In many experiments (not included in the table) depolarization reduced cell-to-cell diffusion to such an extent that no $F2$ rise was detectable, and hence a determination of k_J was not possible. This was especially true for the larger molecules, LRB-Leu_3Glu_2 and FTU-sugar, whose rates of cell-to-cell diffusion were very low, even at resting potential. For example, the rate constants computed for FTU-sugar in the experiment of Fig. 11 (injection #6 in Table 2) are k_J = 0.42, k_L = 0.67, k_S = 1.0 (10^{-3} sec^{-1}). It was therefore not feasible to use these tracers for studies of reduction in junctional permeability by depolarization.

[1] In injection #1, the change from 2 to 61 mM K^+ reduced k_J about twofold, whereas in injection #7, a change from 2 to 33 mM K^+ reduced k_J more than tenfold. This does not indicate that depolarization has selectively affected junctional permeability to CO-TMR. Membrane potential is but one regulator of cell-to-cell channels in this tissue, with cytoplasmic *p*Ca and pH setting the range over which junctional conductance responds to changes in potential (Obaid et al., 1983); injections #7*a* and *b* may have been into a cell whose *p*Ca and/or pH was lower than in the cell of injections #1*a* and *b*.

Table 2. Constancy of k_J ratio for a tracer pair

Injection #	Co-injected tracers	$[K^+]_o$ (mM)	$k_J \times 10^3$ (sec^{-1})	k_J ratio for tracer pair
1*a*	CO-F	2	8.67	2.89
	LRB-Glu-Tyr-Glu		3.0	
1*b*	CO-F	61	4.0	2.89
	LRB-Glu-Tyr-Glu		1.38	
2	CO-F	5	3.83	2.88
	LRB-Glu-Tyr-Glu		1.33	
3[a]	CO-F	5	5.33	3.20
	LRB-Glu-Tyr-Glu		1.67	
4	CO-F	2	9.17	6.88
	LRB-Leu_3-Glu_2		1.33	
5	CO-F	2	8.33	7.14
	LRB-Leu_3-Glu_2		1.17	
6	CO-TMR	2	5.83	14.0
	FTU-sugar		0.42	
7*a*	CO-TMR	2	5.0	—
	—		—	
7*b*	CO-TMR	33	0.33	—
	—		—	

[a] These data from an injection into one cell of an isolated pair; all others from gland preparations.

E. Comparison of Cell-to-Cell Conductance and Tracer Permeability

The foregoing results showed no evidence of a change in channel selectivity upon depolarization. However, it was entirely possible that the molecules in our repertoire, useful for probing the channel in this respect (CO-F, CO-TMR, LRB, LRB-Glu-Tyr-Glu) did not differ enough in size to discriminate between different channel open states. Therefore, with junctional conductance measurements, we extended the analysis to small inorganic ions that carry electrical current from cell-to-cell through the junctions.

We clamped both cells of isolated pairs to the same voltage while measuring cell-to-cell tracer (CO-F) diffusion and the electrical conductance, g_J, of the junction. To derive k_J, the model here was a system of two compartments (cells), as described in the Appendix. A result is illustrated in Fig. 12 where *A* gives plots of $F1$, $F2$ and g_J on the same time base, with membrane potentials clamped at −31 mV throughout, and *B* gives such plots for a second injection into the same cell, with membrane potentials clamped to −75 mV. It is evident that both junctional conductance and cell-to-cell tracer diffusion were enhanced by hyperpolarization: g_J rose, and the rates of $F1$ decay and $F2$ rise increased.

The k_J's necessary for a fit of the theoretical curves (Fig. 12*A* and *B*, solid lines) to both sets of fluorescence data suggest that the enhancements of k_J and g_J were proportional: both k_J and g_J approximately doubled on increasing the resting potential. This proportionality of k_J and g_J is further illustrated in Fig. 12*C* in which the results obtained from four cell pairs are pooled. Not only are the changes in k_J and g_J from a given junction proportional (identical symbols), but all the data fall on a straight line. Thus, cell-to-cell diffusion of the small inorganic ions and of the much larger CO-F molecules is equally affected by membrane potential. And, here too, the permeability ratio for large and small junction permeant (i.e., k_J/g_J) is conserved in the various cell junctions, even though the absolute values may differ. This echoes the earlier result of the constancy of the k_J ratio of two tracers, obtained from experiments on cell chains, and it strengthens our confidence in the adequacy of the compartment model.

Cell-to-cell diffusion in isolated cell pairs was in general much poorer than in glands, as indicated by the much lower k_J values for CO-F. This difference may reflect a decrease in intracellular *p*Ca or pH, or a loss of cell-to-cell channels resulting from the cell pair isolation procedures. At any rate, this reduced permeability limited the choice of tracer for the study of k_J/g_J comparison to CO-F, because even at the most negative membrane potentials, the larger tracers' cell-to-cell diffusion was close to the limit of our resolution.

Extrapolation of the g_J *versus* k_J curve in Fig. 12*C* to k_J values derived for CO-F in the gland, e.g., 8.7×10^{-3} sec^{-1} of Fig. 8*A*, would imply a g_J of about 30 μS between cells in the gland—an entirely possible value because such a conductance has on occasion been seen in cell pairs (Obaid et al., 1983).

The rate constant k_J can be converted to a more general permeability parameter, $P_c = k_J V$, where V is the average cell volume, and P_c can be described as the rate of clearance of tracer from one cell to another. We can then express the general relationship between carboxyfluorescein permeability and junctional conductance as the ratio P_c/g_J. Using the data in Fig. 12*C* and assuming an average cell volume of approximately 3.5×10^{-7} cm^3, P_c/g_J is about 1×10^{-4} $\Omega cm^3 sec^{-1}$. This ratio is independent of the exact cellular geometry and number of channels in a junction and can be scaled by the appropriate k_J ratios to describe other junction permeants.

Discussion

The rate of cell-to-cell transfer of molecules in junction-connected systems depends on at least three diffusion processes: diffusion through cytoplasm, through (nonjunctional) cell membrane, and through cell-to-cell channels. The present results show that all three, in fact, are significant determinants of the kinetics of cell-to-cell diffusion and that sequestration by cytoplasmic elements can be a significant factor in addition. Diffusibility through cell-to-cell junctions varied inversely with tracer size

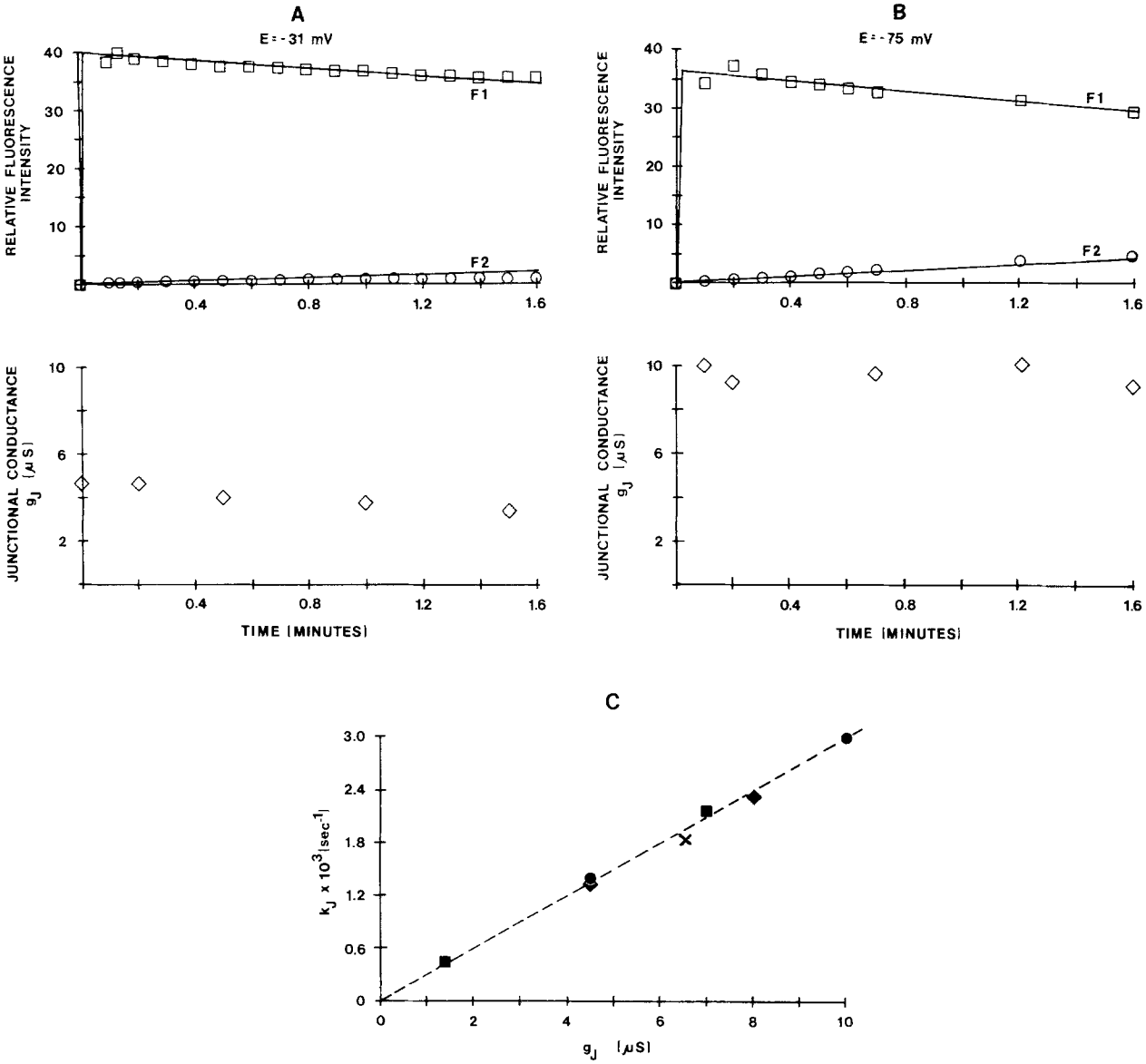

Fig. 12. Comparison of cell-to-cell tracer diffusion with junctional conductance. Effects of membrane potential. Cell pair in TC-199 MK medium after isolation by collagenase treatment. A double voltage clamp is used to set both cells' membrane potentials and to measure junctional conductance. (*A*): Fluorescence (squares: *F*1; circles: *F*2) and junctional conductance (g_J: diamonds) for a CO-F injection with cells clamped at −31 mV throughout. (*B*): Data for a second CO-F injection with membrane potentials at −75 mV throughout. The usual fast initial phase of *F*1 decay is absent in these records because the site of injection was somewhat distant from the recording region (*see* Fig. 7). Curves for the fluorescence data were generated using the two-cell compartment model (*see* Appendix). Rate constants k_J, k_L, k_S (10^{-3} sec^{-1}) for *A*: 1.4, 1.0, 1.0; for *B*: 3.0, 1.0, 1.0. The bottom graph (*C*) shows a plot of k_J *vs.* g_J from four different junctions. In this graph identical symbols denote measurements taken on the same junction. The filled circles are the data from *A* and *B*. Dashed line fitted by eye

and was shown to be altered by cell membrane potential, in a manner consistent with a regulation mechanism in which the number of open channels changes, but not the channel pore size or selectivity.

A. Cytoplasmic Diffusion

Diffusibility of the tracers in cytoplasm does not simply depend on tracer size. In agar, diffusion of LRB (mol wt 559) was 1.3 times slower than that of CO-F (mol wt 376), but in cytoplasm, it was 2.4 times slower. A possible reason for this surprisingly low cytoplasmic mobility of LRB is the presence of two SO_3^- groups, which may favor its sequestration or binding to cytoplasmic components. LRB conjugated to Glu-Tyr-Glu has only one such group, and, although considerably larger than LRB, it has about the same cytoplasmic diffusibility as LRB. And fit-

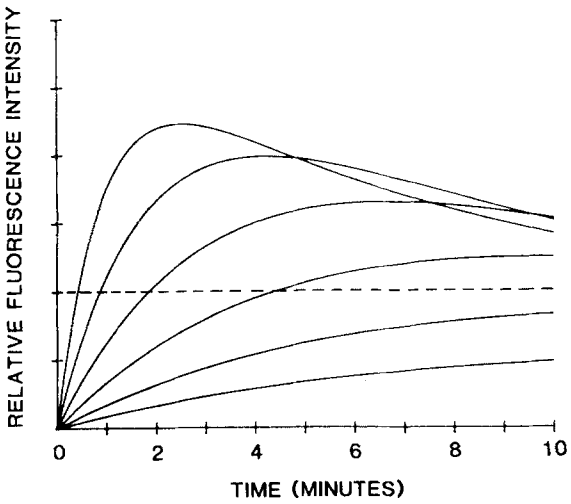

Fig. 13. Family of theoretical $F2$ curves generated by changing k_J in the (five-cell) compartment model (*see* Appendix). k_J is successively reduced, from top curve to bottom, by a factor of two: 8.67, 4.33, 2.17, 1.08, 0.54, 0.27×10^{-3} sec^{-1}. For each curve, the amount of tracer injected is the same, and $k_L = 0.83 \times 10^{-3}$ sec^{-1}, $k_S = 0$. The dashed line is the estimated threshold for visual tracer detection; its intersection with the curves gives the "transit time"

tingly, CO-TMR, which in other respects is quite like LRB (*see* Fig. 2) but has COO^- groups in place of the SO_3^- groups, diffuses only 1.2 times more slowly in cytoplasm than does CO-F.

The important point with respect to our analysis of cell-to-cell diffusion is, however, that despite these differences, intracellular diffusion of all the tracers used was fast enough never to be rate-limiting in the cell-to-cell transfer.

B. Loss and Sequestration of Tracers

The rate of loss from the cells depended on the tracer, and there was some indication that the sequestration rate did as well, as one might expect. In experiments on junctional transfer it became clear that the rates of loss and sequestration were not negligible compared to the rate of cell-to-cell diffusion. When the rate constants for loss and/or sequestration were similar to or larger than the rate constant for cell-to-cell diffusion, the cell-to-cell channels no longer were the rate-limiting factor for cell-to-cell transfer. Hence, estimates of relative junctional permeabilities, or changes therein, cannot safely be based simply on comparisons of the fluorescence gradient between the injected cell and its neighbor, or on comparisons of the rates of rise of fluorescence intensity in the neighboring cell.

C. Cell-to-Cell Tracer Diffusion and Regulation of Cell-to-Cell Channel Closure

At cell resting potential, the rate constants, k_J, were inversely related to tracer size but not to charge (Table 1; *see also* Fig. 14). Depolarization produced a reversible reduction in these rate constants. This result is consistent with the earlier finding that junctional conductance, g_J, decreases upon depolarization (Obaid et al., 1983). We show here that the changes in k_J for large and small tracers and in g_J are proportional. The simplest interpretation of this result is that depolarization affects junctional permeability by reducing the number of open channels, but not by changing their effective pore diameter or selectivity.

However, this result does not rule out that the cell-to-cell channel has more than one open, conducting state. (We consider here only open states that differ in selectivity and not those that differ just in kinetic properties.) First, such states might be too short-lived or too infrequent to be detected by our method. (With single-channel recording techniques, multiple conductance states have been observed to occur, with low probability, in nonjunctional membrane channels; *see* Hamill & Sakmann, 1981; Sachs, 1983). Second, multiple open states may become manifest under conditions of junctional permeability modulation other than depolarization. One such condition was thought to be elevation of cytosolic $[Ca^{2+}]$ (Rose et al., 1977), as may well be. However, our warning from the preceding section applies also for the experiments from which this conclusion was drawn. It was drawn, based on a comparison between measurements of transit time through cell junctions (i.e., the period from injection of tracer to its detection in an adjacent cell) of different-sized tracers at low and high cytosolic $[Ca^{2+}]$: Ca^{2+} induced a prolongation of transit time that was disproportionately greater for the larger molecules than for the smaller ones. The present analysis makes this conclusion no longer compelling. When junctional permeability is low, as in the case of the larger tracers, the loss or sequestration rate may become dominant and transit times may become disproportionately prolonged compared to those of smaller molecules.

A graphic illustration of this effect is given in the theoretical curves of Fig. 13. These represent changes in fluorescence intensity in a cell adjacent to an injected one (five-cell chain). The dashed line designates an assumed visual threshold for tracer detection, corresponding to that in the described setup. For the top curve, k_J is 8.67×10^{-3} sec^{-1} and for each successive curve, k_J is reduced by a factor

of two, whereas the other parameters (k_L, k_S, amount of tracer injected) are held constant. With each reduction in k_J, the approach to threshold becomes less linear and the increase in transit time less proportional to the k_J reduction. Closing half the channels in a junction may thus increase transit time twofold for a small tracer with an initial k_J of 8 $\times$ 10^{-3} sec^{-1}, but increase it manifold for a large tracer with an initial k_J of 1 $\times$ 10^{-3} sec^{-1}. For the two bottom curves, threshold is, in fact, never reached because the loss rate constant now has become dominant. (In calculating these curves, k_S was set at 0; sequestration would enhance the nonproportional relation between k_J and transit time.)

D. Channel Selectivity: Effective Pore Diameter

The constancy of the permeability ratio of paired, different-sized permeants in junctions of quite different absolute permeabilities (Table 2 and Fig. 12) suggests that there is only one type of cell-to-cell channel in these cells and that all open cell-to-cell channels exhibit the same selectivity. Furthermore, it is evident from Table 1 that, for the permeants studied here, molecular size, but not net negative charge of the permeant, is a major determinant for k_J (but *see* Flagg-Newton, Simpson & Loewenstein, 1979, and Brink & Dewey, 1980, for other cell-to-cell channels and permeants). Thus selectivity, as measured by k_J, seems here to be based mainly on the size relation of permeant mean diameter to channel pore diameter rather than on a particular charge or molecular configuration of the permeant.

If one considers the cell-to-cell channel as a cylinder filled with stationary viscous liquid, and a tracer molecule as a sphere whose diameter is its mean diameter as defined in Table 1, one can estimate the channel diameter based on the tracers' relative k_J values (i.e., permeabilities) and a hydrodynamic theory for the permeability P to spheres moving through such a cylinder (Faxén, 1922; Haberman & Sayre, 1958). The theory assumes no charge interactions between sphere and cylinder wall but it accounts for friction and drag of a sphere moving through the cylinder. We calculate the relative permeabilities P of a cylinder of radius R for spheres of increasing radius A and compare the predicted relation of P and sphere diameter for a given cylinder radius with the relation of k_J and tracer mean diameter.

$$P = 117(1-\alpha)^2 \frac{(1 - 2.105\alpha - 2.0865\alpha^3 - 1.7068\alpha^5 - 0.72603\alpha^6)}{1 - 0.75857\alpha^5}$$

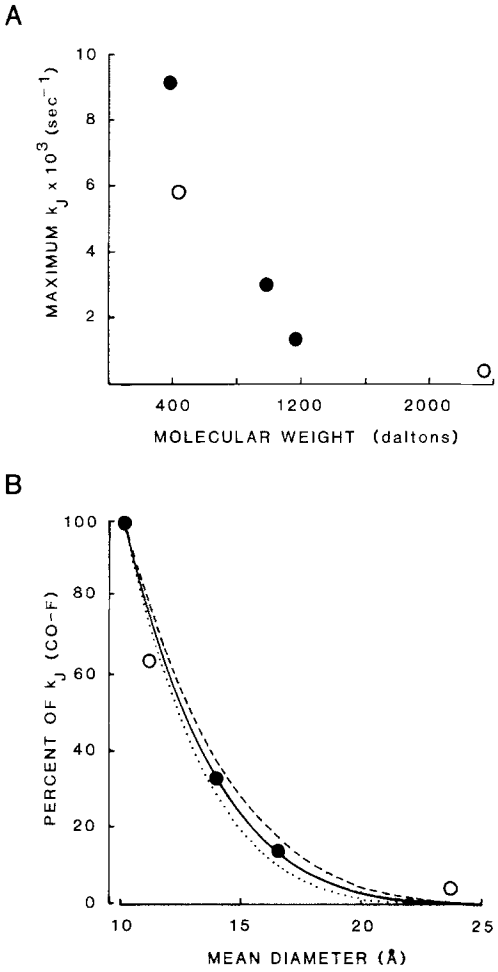

Fig. 14. Dependence of k_J on tracer size. (*A*): Highest k_J values obtained for each tracer, plotted against tracer molecular weight (data from Table 2). (*B*): k_J values relative to k_J for CO-F as a function of tracer mean diameter (from Table 1). Closed circles from experiments in which CO-F was one of the two co-injected tracers (injections 1*a*, 2–6 from Table 2). Open circles represent the k_J's (relative to maximum k_J for CO-F) for CO-TMR and co-injected FTU-sugar (injection #6, Table 2). Note that in this case, CO-F was not co-injected and therefore these data cannot be directly included for comparison with the theoretical curve

where α is the ratio of sphere to cylinder radius, A/R. (Equation and constants are from Dwyer, Adams & Hille, 1980.) Figure 14*B* gives a plot of the tracers' k_J values relative to that of the smallest tracer, CO-F, as a function of tracer mean diameter, and three theoretical curves representing P, calculated for a cylinder of 27, 29 and 31 Å diameter (dotted, solid and dashed line, respectively). The curve for a 29 Å diameter most closely describes the relative k_J's of the three tracers that can be directly compared (filled circles; *see* figure legend).

Thus, the earlier estimate of the permeation

limiting channel diameter of 21–30 Å for insects (Schwarzmann et al., 1981) sharpens to 29 Å.

This paper is based in part on portions of Dr. Zimmerman's dissertation presented to the University of Miami in partial fulfillment of the requirement for the degree of Doctor of Philosophy.

We are grateful to Drs. E.F. Barrett, K.L. Magleby, W. Nonner and B.S. Pallotta for their generous help with the dissertation work; to Prof. W.R. Loewenstein for many helpful discussions and suggestions regarding the manuscript; and to Mrs. S. Brill for her excellent typing of the manuscript.

This work was supported by NIH grant No. 5R01 CA14464.

References

Brink, P.R., Dewey, M.M. 1980. Evidence for fixed charge in the nexus. *Nature (London)* **285:**101–102

Dahl, G., Isenberg, G. 1980. Decoupling of heart muscle cells: Correlation with increased cytoplasmic calcium activity and with changes of nexus ultrastructure. *J. Membrane Biol.* **53:**63–75

Dwyer, T.M., Adams, D.J., Hille, B. 1980. The permeability of the endplate channel to organize cations in frog muscle. *J. Gen. Physiol.* **75:**469–492

Faxén, H. 1922. Die Bewegung einer starren Kugel längs der Achse eines mit zäher Flüssigkeit gefüllten Rohres. *Ark. Mat. Astron. Fysik.* **17:**1–28

Flagg-Newton, J., Simpson, I.N., Loewenstein, W.R. 1979. Permeability of the cell-to-cell membrane channels in mammalian cell junction. *Science* **205:**404–407

Haberman, W.L., Sayre, R.M. 1958. Motion of rigid and fluid spheres in stationary and moving liquids inside cylindrical tubes. *In:* David Taylor Model Basin (Dept. of the Navy), Report 1143. U.S. Department of Defense, Navy Department, Washington, D.C.

Hamill, O.P., Sakmann, B. 1981. Multiple conductance states of single acetylcholine receptor channels in embryonic muscle cells. *Nature (London)* **294:**462–464

Harris, A.L., Spray, D.C., Bennett, M.V.L. 1981. Kinetic properties of voltage-dependent junctional conductance. *J. Gen. Physiol.* **77:**95–117

Kehl, T.H., Moss, C., Dunkel, J. 1975. LM²—a logic machine minicomputer. *I.E.E.E. Comp.* **8:**12–22

Loewenstein, W.R. 1981. Junctional intercellular communication: The cell-to-cell membrane channel. *Physiol. Rev.* **61:**829–913

Loewenstein, W.R., Kanno, Y., Socolar, S.J. 1978. Quantum jumps of conductance during formation of membrane channels at cell-cell junction. *Nature* **274:**133–136

Metzger, P., Weingart, R. 1984. Electric current flow in a two-cell preparation from *Chironomus* salivary glands. *J. Physiol. (London)* **346:**599–619

Obaid, A.L., Rose, B. 1981. Junctional resistance of *Chironomus* cell pairs depends on (nonjunctional) membrane potential. *Biophys. J.* **33:**106*a*

Obaid, A.L., Socolar, S.J., Rose, B. 1983. Cell-to-cell channels with two independently regulated gates in series: Analysis of junctional conductance modulation by membrane potential, calcium, and pH. *J. Membrane Biol.* **73:**69–89

Oliveira-Castro, G.M., Loewenstein, W.R. 1971. Junctional membrane permeability: Effects of divalent cations. *J. Membrane Biol.* **5:**51–77

Riggs, D.S. 1963. The Mathematical Approach to Physiological Problems. pp, 193–220. M.I.T. Press. Cambridge (Mass.)—London (England)

Rose, B. 1970. Junctional membrane permeability: Restoration by repolarizing current. *Science* **169:**607–609

Rose, B. 1971. Intercellular communication and some structural aspects of membrane junctions in a simple cell system. *J. Membrane Biol.* **5:**1–19

Rose, B., Loewenstein, W.R. 1975. Permeability of cell junction depends on local cytoplasmic calcium activity. *Nature (London)* **254:**250–252

Rose, B., Loewenstein, W.R. 1976. Permeability of a cell junction and the local cytoplasmic free ionized calcium concentration: A study with aequorin. *J. Membrane Biol.* **28:**87–119

Rose, B., Rick, R. 1978. Intracellular pH, intracellular free Ca, and junctional cell-cell coupling. *J. Membrane Biol.* **44:**377–415

Rose, B., Simpson, I., Loewenstein, W.R. 1977. Calcium ion produces graded changes in permeability of membrane channels in cell junction. *Nature (London)* **267:**625–627

Sachs, F. 1983. Is the acetylcholine receptor a unit conductance channel? *In:* Single Channel Recordings. B. Sakman and E. Neher, editors. pp. 365–376. Plenum, New York

Schwarzmann, G., Wiegandt, H., Rose, B., Zimmerman, A., Ben-Haim, D., Loewenstein, W.R. 1981. Diameter of the cell-to-cell junctional channels as probed with neutral molecules. *Science* **213:**551–553

Simpson, I., Rose, B., Loewenstein, W.R. 1977. Size limit of molecules permeating the junctional membrane channels. *Science* **195:**294–296

Socolar, S.J., Politoff, A.L. 1971. Uncoupling cell junctions of a glandular epithelium by depolarizing current. *Science* **172:**492–494

Spray, D.C., Harris, A.L., Bennett, M.V.L. 1979. Voltage dependence of junctional conductance in early amphibian embryos. *Science* **204:**432–434

Spray, D.C., Harris, A.L., Bennett, M.V.L. 1981*a*. Gap junctional conductance is a simple and sensitive function of intracellular pH. *Science* **211:**712–714

Spray, D.C., Harris, A.L., Bennett, M.V.L. 1981*b*. Equilibrium properties of a voltage-dependent junctional conductance. *J. Gen. Physiol.* **77:**77–93

Turin, L., Warner, A. 1977. Carbon dioxide reversibly abolishes ionic communication between cells of early amphibian embryo. *Nature (London)* **270:**56–57

Turin, L., Warner, A.E. 1980. Intracellular pH in early *Xenopus* embryos: Its effect on current flow between blastomeres. *J. Physiol. (London)* **300:**489–504

Received 23 October 1984

Appendix

Compartment Model for Cell-to-Cell Diffusion

Cells are represented as identical, interconnected compartments in series (Fig. 9), and cell-to-cell transfer, irreversible loss, and sequestration of tracers as linear, first order processes; sequestered tracer molecules contribute to fluorescence. For simplicity, intracellular diffusion of tracer from the injection site was not included in the model (*see* p. 275). To simulate cell-to-cell diffusion data obtained from cells within glands, it was generally sufficient to represent the gland as a chain of five cells (Fig. 9*B*); that is, for the time span of these simulations, additional compartments did not significantly change the theoretical curves.

The following parameters were used to describe the system:

C_n, relative free tracer concentration in compartment n, where $n = 1$ or 2 for the isolated cell pair model, and 1, 2, 3, 4, or 5 for the gland (five-cell chain) model.

S_n, relative concentration of sequestered (but fluorescent) tracer molecules in the subcompartment of compartment n.

F_n, relative fluorescence intensity in compartment n; i.e., concentration of fluorescent tracer molecules in compartment n, where $F_n = C_n + S_n$. To simulate isolated cell pair data, F_1 and F_2 were plotted against time; and for the data from a gland, F_3 and F_4 were plotted against time.

k_J, rate constant for reversible intercompartmental transfer of free tracer molecules, the parameter representing junctional permeability.

k_L, rate constant for irreversible loss of tracer (or fluorescence) from each compartment.

k_S, rate constant for irreversible sequestration of tracer within each compartment.

V, volume of each compartment, set at 1 unit. Preparations were chosen such that all cells within the five-cell chain had approximately the same linear dimensions.

I, relative amount of tracer injected.

Initial concentrations in all compartments were assumed to be zero. To simulate tracer injection, C_1 (for the isolated cell pair) or C_3 (for the gland) was instantaneously stepped to I/V. Thereafter, changes in tracer concentration and fluorescence intensity were described by the following differential equations:

for the isolated cell pair (Fig. 9*A*),

$$\frac{dC_1}{dt} = k_J (C_2 - C_1) - k_L C_1 V_1 - k_S C_1 V_1$$

$$\frac{dC_2}{dt} = k_J (C_1 - C_2) - k_L C_2 V_2 - k_S C_2 V_2$$

for $n = 1, 2$:

$$\frac{dS_n}{dt} = k_S C_n V_n$$

$$F_n = C_n + S_n$$

and for cells within a gland (Fig. 9*B*),

$$\frac{dC_1}{dt} = k_J (C_2 - C_1) - k_L C_1 V_1 - k_S C_1 V_1$$

$$\frac{dC_2}{dt} = k_J (C_1 + C_3 - 2C_2) - k_L C_2 V_2 - k_S C_2 V_2$$

$$\frac{dC_3}{dt} = k_J (C_2 + C_4 - 2C_3) - k_L C_3 V_3 - k_S C_3 V_3$$

$$\frac{dC_4}{dt} = k_J (C_3 + C_5 - 2C_4) - k_L C_4 V_4 - k_S C_4 V_4$$

$$\frac{dC_5}{dt} = k_J (C_4 + C_5) - k_L C_5 V_5 - k_S C_5 V_5$$

for $n = 1$ to 5:

$$\frac{dS_n}{dt} = k_S C_n V_n$$

$$F_n = C_n + S_n.$$

These simultaneous differential equations were solved by numerical methods using an LM^2 (Kehl, Moss & Dunkel, 1975) or a PDP-11 computer. Initial estimates of the rate constants were obtained from semilogarithmic plots of the fluorescence data ($F1$ decays).